The T#2-$Li_{2/3}Co_{2/3}Mn_{1/3}O_2$ System. 1. Its Structural Characterization

F. Tournadre,† L. Croguennec,*,† I. Saadoune,†,‡ F. Weill,† Y. Shao-Horn,†,§ P. Willmann,|| and C. Delmas†

Institut de Chimie de la Matière Condensée de Bordeaux−CNRS and Ecole Nationale Supérieure de Chimie et Physique de Bordeaux, Université Bordeaux I, 87 Av. du Dr A. Schweitzer, 33608 Pessac Cedex, France, L.C.M.E., Département de Chimie, Faculté des Sciences et Techniques, Av. Abdelkrim, B.P. 549, 40000 Marrakech, Morocco, Department of Mechanical Engineering, 3-342 A, Massachusetts Institute of Technology, 77 Massachusetts Avenue, Cambridge, Massachusetts 02139, and Centre National d'Etudes Spatiales, 18 Av. Edouard Belin, 31401 Toulouse Cedex 4, France

Received November 17, 2003

The layered T#2-$Li_{2/3}Co_{2/3}Mn_{1/3}O_2$ phase was obtained by ion exchange in molten salts of Na^+ by Li^+ in P2-$Na_{2/3}Co_{2/3}Mn_{1/3}O_2$. X-ray photoelectron spectroscopy (XPS) analyses have shown that cobalt and manganese ions are present in T#2-$Li_{2/3}Co_{2/3}Mn_{1/3}O_2$ at the trivalent and tetravalent oxidation states, respectively. The refinement of the neutron diffraction data was achieved, and the structure was described in the *Cmca* space group with two $Co_{2/3}Mn_{1/3}O_2$ slabs per unit cell. Thanks to nuclear density Fourier difference maps calculations, it was shown that the lithium ions are distributed in the 8e and $8f_{edges}$ tetrahedral sites. Transmission electron microscopy has shown no evidence of lithium ordering in the interslab space.

Introduction

O2-$LiCoO_2$ was the first metastable lithiated phase obtained, a long time ago, by a sodium by lithium ion-exchange reaction.[1] Note that all the phases will be named in this paper according to the packing designation commonly used for the layered oxides: the letters P, T, and O describe the alkali ion environment (prismatic, tetrahedral, or octahedral, respectively) and the numbers 1, 2, 3, etc. give the number of slabs required to describe the hexagonal cell.[2] Recently, the O2-$LiCoO_2$ system was reinvestigated by Dahn's group and in our laboratory,[3,4] we focused our interest on the structural characterization by neutron diffraction[5] and on the transmission electron microscopy study[6] of the various phases obtained upon cycling, especially the T#2-Li_x-CoO_2 ($0.52 < x \leq 0.72$).

Dahn et al. were first interested in O2-type systems because they had shown that O2-$LiMnO_2$, contrary to O3-$LiMnO_2$, did not convert to spinel upon cycling.[7] They focused their interest on the T#2-$Li_{2/3}[Ni_{1/3}Mn_{2/3}]$-$O_2$ phase and showed that its electrochemical performances were limited because only 1/3 lithium ions could be removed from the structure.[8,9] Finally, they studied also cobalt-substituted phases, such as the $Li_{2/3}[Ni_{1/3-x}Co_xMn_{2/3}]O_2$ phases ($0 < x \leq 1/3$)[10] and the $Li_{2/3}[Ni_{1/3-x/2}Co_xMn_{2/3-x/2}]O_2$ phases ($0 < x \leq 2/3$); in this latter system, all the manganese ions were tetravalent.[11] For these two series of compounds, it appears that the better electrochemical performances were obtained for the materials with the higher cobalt contents. Note also that only a few well-crystallized phases were obtained by ion-exchange reaction: O2-$LiCoO_2$,[3,4] T#2-$Li_{2/3}[Ni_{1/3}Mn_{2/3}]O_2$,[12] and T#2-$Li_{2/3}[Co_{2/3}$-$Mn_{1/3}]O_2$.[11] All the other phases, O2-$LiMnO_2$,[7] O6−$Li_{2/3}[Mg_{0.30}Mn_{0.70}]O_2$,[13] $Li_{2/3}[Ni_{1/3-x}Co_xMn_{2/3}]O_2$, and $Li_{2/3}[Ni_{1/3-x/2}Co_xMn_{2/3-x/2}]O_2$, were more or less stacking faulted structures.[14]

The P2-$Na_{2/3}Co_{2/3}Mn_{1/3}O_2$ precursor has an AB BA oxygen packing, with the sodium ions in prismatic environments between two slabs of edge-sharing MO_6 octahedra. During ionic exchange, as shown in Figure 1, the T#2 structure is obtained by the translation of

* Corresponding author. Tel.: +33-5-4000-2234. Fax: +33-5-4000-6698. E-mail: crog@icmcb.u-bordeaux.fr.
† Université Bordeaux I.
‡ L.C.M.E.
§ Massachusetts Institute of Technology.
|| Centre National d'Etudes Spatiales.

(1) Delmas, C.; Braconnier, J. J.; Hagenmuller, P. *Mater. Res. Bull.* **1982**, *17*, 117.
(2) Delmas, C.; Fouassier, C.; Hagenmuller, P. *Physica* **1980**, *99B*, 81.
(3) Paulsen, J. M.; Mueller-Neuhaus, J. R.; Dahn, J. R. *J. Electrochem. Soc.* **2000**, *147*, 508−516.
(4) Carlier, D.; Saadoune, I.; Suard, E.; Croguennec, L.; Ménétrier, M.; Delmas, C. *Solid State Ionics* **2001**, *144*, 263−276.
(5) Carlier, D.; Croguennec, L.; Ceder, G.; Ménétrier, M.; Shao-Horn, Y.; Delmas, C. *Inorg. Chem.* **2004**, *43* (3), 914−922.
(6) Shao-Horn, Y.; Weill, F.; Croguennec, L.; Carlier, D.; Ménétrier, M.; Delmas, C. *Chem. Mater.* **2003**, *15*, 2977−2983.
(7) Paulsen, J. M.; Thomas, C. L.; Dahn, J. R. *J. Electrochem. Soc.* **1999**, *146*, 3560.
(8) Paulsen, J. M.; Thomas, C. L.; Dahn, J. R. *J. Electrochem. Soc.* **2000**, *147*, 861−868.
(9) Lu, Z. H.; Dahn, J. R. *J. Electrochem. Soc.* **2001**, *148*, A710.
(10) Lu, Z. H.; Dahn, J. R. *J. Electrochem. Soc.* **2001**, *148*, A237.
(11) Lu, Z. H.; Donaberger, R. A.; Thomas, C. L.; Dahn, J. R. *J. Electrochem. Soc.* **2002**, *149*, A1083−A1091.
(12) Paulsen, J. M.; Thomas, C. L.; Dahn, J. R. *J. Electrochem. Soc.* **2000**, *147*, 2862−2867.
(13) Paulsen, J. M.; Donaberger, R. A.; Dahn, J. R. *Chem. Mater.* **2000**, *12*, 2257−2267.
(14) Lu, Z. H.; Dahn, J. R. *Chem. Mater.* **2001**, *13*, 2078.

10.1021/cm035176p CCC: $27.50
Published on Web 03/16/2004

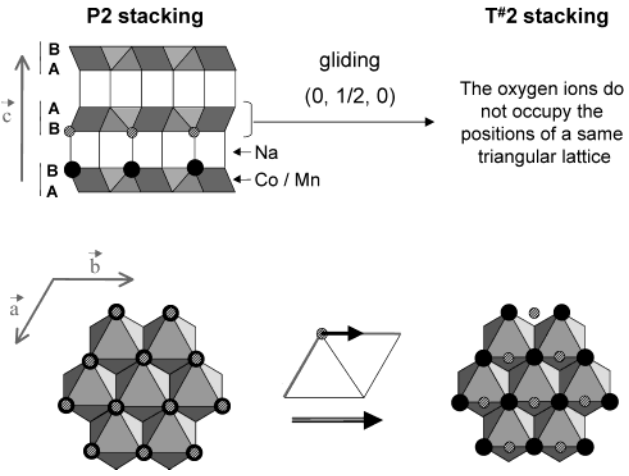

Figure 1. Sheet gliding involved in the P2 → T#2 transformation occurring during the ion-exchange process, as seen from the (110) section and from a top view of the interslab space (only the A, B and B oxygen layers are represented). The oxygen layers at the bottom (dark circles) and at the top (hatched circles) of one interlayer space are highlighted.

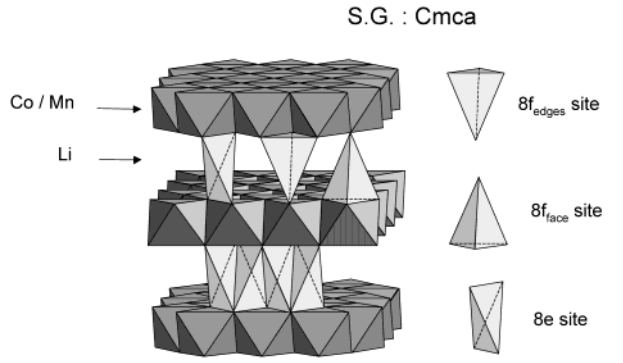

Figure 2. T#2 stacking of $Li_{2/3}Co_{2/3}Mn_{1/3}O_2$. The different distorted tetrahedral sites available for the lithium ions are also displayed.

one slab over two by (0, $^1/_2$, 0). The view of the P2 structure in the (110) section plane is presented on the top of Figure 1 and the two oxygen layers of one interslab space are highlighted: the lower one with black circles and the upper one with hatched circles. After the structural transition and, therefore, after the translation of the top oxygen layer, the oxygen ions do not occupy anymore the positions of a same triangular lattice: unusual tetrahedral environments are formed in the interslab space for lithium ions. The perspective of the T#2 structure is represented along the $c_{orth.}$ axis in Figure 2. The cobalt and manganese ions are distributed in the 4a (0, 0, 0) position of the *Cmca* orthorhombic space group and the oxygen ions in an 8f (0, ∼0.83, ∼0.60) position. Three different lithium sites are available for lithium in the interslab space. The $(LiO_4)_{8e}$ tetrahedra are highly distorted; they share one edge on each side with MO_6 octahedra (Figure 2). Two other kinds of tetrahedral sites, corresponding to 8f positions, are available. The first one, noted 8f$_{edges}$, shares three edges with three MO_6 octahedra on one side and a corner with three MO_6 octahedra on the other side. The second one, noted 8f$_{face}$, shares on one side a corner with three MO_6 octahedra and, on the other side, a face with one MO_6 octahedron. Note that the lithium ions are not expected to be stabilized in the 8f$_{face}$ site because of face-sharing with MO_6 octahedra and thus short $M^{n+}-Li^+$ distances. Paulsen et al. always only considered the occupancy of the 8e sites by lithium in T#2-type structures, and no evidence of 8f$_{face}$ occupancy was found experimentally by some of us for the T#2-$Li_{0.56}CoO_2$ phase.[5] But, recently, for Li//Li_xCoO_2 Carlier et al. needed to introduce lithium in the 8f$_{edges}$ sites to obtain by first-principles ab initio calculations a minimization of the energy of the structures and a calculated $V = f(x)$ curve in good agreement with the experimental one.[15]

In this paper (part 1), we present the structure determination of the T#2-$Li_{2/3}Co_{2/3}Mn_{1/3}O_2$ phase, with especially the localization of the lithium ions in the interslab space. In the companion paper (part 2), the results related to its electrochemical performances in lithium cells are reported.

Experimental Section

Material Preparation. The Na_xCoO_2 phases exhibit the P2-stacking for $0.64 < x < 0.74$.[16] We chose the $x = 2/3$ intermediate composition to prepare the P2-$Na_{2/3}Co_{2/3}Mn_{1/3}O_2$ precursor phase by analogy with P2-Na_xCoO_2. P2-$Na_{2/3}Co_{2/3}Mn_{1/3}O_2$ was synthesized by the coprecipitation method. A solution of transition metal nitrates (2/3 of $Co(NO_3)_2{\cdot}6H_2O$ and 1/3 of $Mn(NO_3)_2{\cdot}6H_2O$) was slowly dripped into a NaOH (1 M)−NH_4OH (3 M) solution (with 5% Na in excess) while stirring. The obtained precipitate was first dried under vacuum at 80 °C for 3 h and then dried in air at 120 °C overnight. The precipitate was then ground and heated at 950 °C under O_2 for 12 h. The powder was finally quenched in air.

The lithium-containing phase was prepared from the sodium-containing one by ion exchange of Na^+/Li^+ in molten salts. P2-$Na_{2/3}Co_{2/3}Mn_{1/3}O_2$ was added to a eutectic mixture of $LiNO_3$ and LiCl (88:12, with Li/Na = 7) at 280 °C. After 1 h of reaction, the mixture was cooled; then the product was washed with demineralized water and the $Li_{2/3}Co_{2/3}Mn_{1/3}O_2$ phase was recovered after filtration and drying at 120 °C overnight.

X-ray and Neutron Diffraction. The X-ray diffraction (XRD) patterns of the P2-$Na_{2/3}Co_{2/3}Mn_{1/3}O_2$ and T#2-$Li_{2/3}Co_{2/3}Mn_{1/3}O_2$ phases were collected at room temperature from 5° to 120° (2θ) with an 0.02° step and a 40-s counting time by step, using a Siemens D5000 powder diffractometer with Cu Kα radiation and a graphite diffracted beam monochromator.

Neutron diffraction was performed at the Laue-Langevin Institute at Grenoble (France) on the high-resolution powder D2B diffractometer. The samples were contained in an 8-mm-diameter vanadium tube. The diffraction pattern ($\lambda = 1.5940$ Å) was collected at room temperature from 0° to 162° (2θ) with an 0.05° step and a total counting time of 6 h.

The structural characterization of T#2-$Li_{2/3}Co_{2/3}Mn_{1/3}O_2$ was then carried out by the Rietveld method, using the Fullprof program. The Fourier maps calculations and visualizations were achieved respectively using Fourier and Gfourier programs provided with the Winplotr software package.[17] Because of the geometry of the neutron diffractometer (transmission mode), it was necessary to correct for the absorption, to take into account a decrease of the experimental diffracted intensity compared to the expected one. The correction (through the μR factor in the Fullprof program) is especially necessary for the determination of the atomic displacement parameters and site occupancies that highly depend on the relative intensities of the diffraction lines. μ is the linear absorption coefficient of the sample and is defined as $\mu = (n/V)\Sigma_i n_i \sigma_i$, where n is the number of units in the unit cell, V the cell volume, n_i the

(15) Carlier, D.; Van der Ven, A.; Delmas, C.; Ceder, G. *Chem. Mater.* **2003**, *15*, 2651−2660.

(16) Fouassier, C.; Matejka, G.; Reau, J. M.; Hagenmuller, P. *J. Solid State Chem.* **1973**, *6*, 532.

(17) Rodriguez-Carvajal, J. Laboratoire Léon Brillouin, http://www.llb.cea.fr/fullweb/powder.htm.

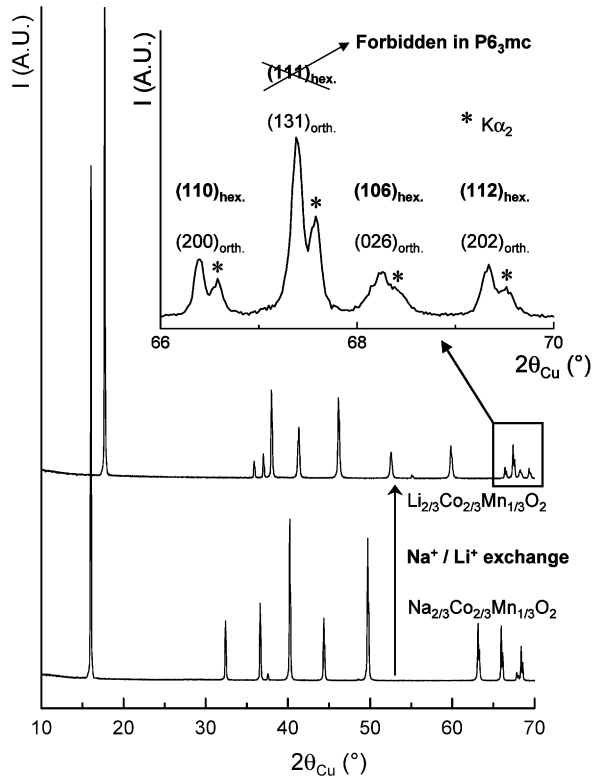

Figure 3. X-ray diffraction patterns of the P2-$Na_{2/3}Co_{2/3}Mn_{1/3}O_2$ and $T^{\#}2$-$Li_{2/3}Co_{2/3}Mn_{1/3}O_2$ phases. An enlargement of the 66°−70° ($2\theta_{Cu}$) range is given in the insert for $T^{\#}2$-$Li_{2/3}Co_{2/3}Mn_{1/3}O_2$: the contribution of the $K\alpha_2$ for Cu radiation leads to a splitting of all the diffraction lines at high 2θ angles, as noted by "*".

number of a given atom in the unit, and σ_i the atomic absorption coefficient for the atom i. R is the radius of the cylinder defined by the sample studied (ϕ = 8 mm). The calculated μR coefficient for the $T^{\#}2$-$Li_{2/3}Co_{2/3}Mn_{1/3}O_2$ phase is 0.79.

Scanning Electron Microscopy. Crystal morphologies of the P2-$Na_{2/3}Co_{2/3}Mn_{1/3}O_2$ and $T^{\#}2$-$Li_{2/3}Co_{2/3}Mn_{1/3}O_2$ phases were analyzed by an Hitachi S-4500 field emission microscope. To avoid charging during the scanning electron microscopy (SEM) analyses, a 2-nm-thick layer of platinum was deposited by cathodic sputtering on powder samples.

X-ray Photoelectron Spectroscopy (XPS). The present XPS data were collected using a VG 220i-XL Escalab spectrometer with a nonmonochromatized Mg Kα source ($h\nu$ = 1253.6 eV) and a diameter for the irradiated area of about 250 μm. The pressure in the analysis chamber during measurements was maintained in the 10^{-7} Pa range. The powder samples were pressed onto small indium foils, and the peaks were recorded with a constant pass energy mode of 20 eV. To quantitatively determine the oxidation states of manganese and cobalt ions, the experimental spectra were fitted by using a Shirley background function and a nonlinear least-squares fitting software provided by VG Scientific. The binding energies were calibrated by fixing the C 1s line of residual carbon at 285 eV with an accuracy of ±0.1 eV.

Electron Diffraction. Electron diffraction patterns were collected from a $T^{\#}2$-$Li_{2/3}Co_{2/3}Mn_{1/3}O_2$ powder sample suspended on a copper grid with lacey carbon under an accelerating voltage of 200 keV on a JEOL 2000FX microscope. Because of the size of the crystals, a microdiffraction mode was used to obtain the diffraction patterns.

Results and Discussion

The $Li_{2/3}Co_{2/3}Mn_{1/3}O_2$ Phase. Figure 3 represents the XRD patterns of the P2-$Na_{2/3}Co_{2/3}Mn_{1/3}O_2$ and $T^{\#}2$-$Li_{2/3}Co_{2/3}Mn_{1/3}O_2$ phases. After 1 h of exchange reaction, the formation of well-crystallized $T^{\#}2$-$Li_{2/3}Co_{2/3}Mn_{1/3}O_2$ was achieved and no evidence of residual P2-$Na_{2/3}Co_{2/3}Mn_{1/3}O_2$ phase was found. The XRD pattern of the lithium-containing phase is typical of a $T^{\#}2$ oxygen packing and can be indexed in the *Cmca* space group with $a_{orth.}$ = 2.8121(4) Å, $b_{orth.}$ = 4.8506(4) Å, and $c_{orth.}$ = 10.006(1) Å. A phase with a $T^{\#}2$ structure has an XRD pattern very similar to that of a phase with an O2 structure:[5,18] the main difference appears around 67° ($2\theta_{Cu}$). Indeed, as shown in the insert in Figure 3, the $(111)_{hex.}$ peak that is observed for the $T^{\#}2$ phase is forbidden in the $P6_3mc$ space group that describes the O2 structure.[18] Note that another small extra diffraction line is observed for a $T^{\#}2$ oxygen packing around 73° ($2\theta_{Cu}$) (the $(113)_{hex.}$ line, not shown here).

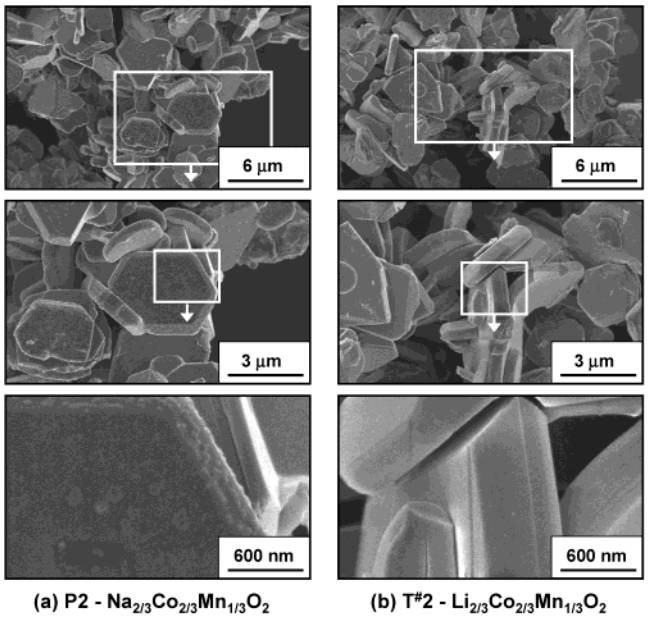

Figure 4. SEM micrographs of the P2-$Na_{2/3}Co_{2/3}Mn_{1/3}O_2$ precursor (a) and $T^{\#}2$-$Li_{2/3}Co_{2/3}Mn_{1/3}O_2$ phase obtained after ion exchange (b).

Scanning Electron Microscopy Analysis. Figure 4 shows scanning electron microscopy micrographs of the P2-$Na_{2/3}Co_{2/3}Mn_{1/3}O_2$ precursor and of the $T^{\#}2$-$Li_{2/3}Co_{2/3}Mn_{1/3}O_2$ phase obtained after ion exchange of sodium by lithium in molten salts. Note that contrary to what is observed for instance for high-temperature layered lithium-containing phases such as $LiNi_{1-y}M_yO_2$,[19,20] the P2-$Na_{2/3}Co_{2/3}Mn_{1/3}O_2$ particles are characterized by a strong anisotropy, with a hexagonal platelike shape. This anisotropy is responsible for preferential orientation of the crystals perpendicular to the *c*-axis, as observed for instance on the X-ray diffraction patterns.[21] These particles have a diameter from 2 to 5 μm and a thickness from 0.5 to 1 μm. On the 600-nm-scale micrographs, some small spherical grains appear all over the surface of the P2-$Na_{2/3}Co_{2/3}Mn_{1/3}O_2$ particles: a small amount of sodium carbonate

(18) Paulsen, J. M.; Dahn, J. R. *J. Electrochem. Soc.* **2000**, *147*, 2478−2485.
(19) Guilmard, M.; Rougier, A.; Grüne, M.; Croguennec, L.; Delmas, C. *J. Power Sources* **2003**, *115*, 305−314.
(20) Pouillerie, C.; Perton, F.; Biensan, P.; Pérès, J.-P.; Broussely, M.; Delmas, C. *J. Power Sources* **2001**, *96*, 293.
(21) Tournadre, F.; Croguennec, L.; Willmann, P.; Delmas, C. *J. Solid State Chem.*, submitted.

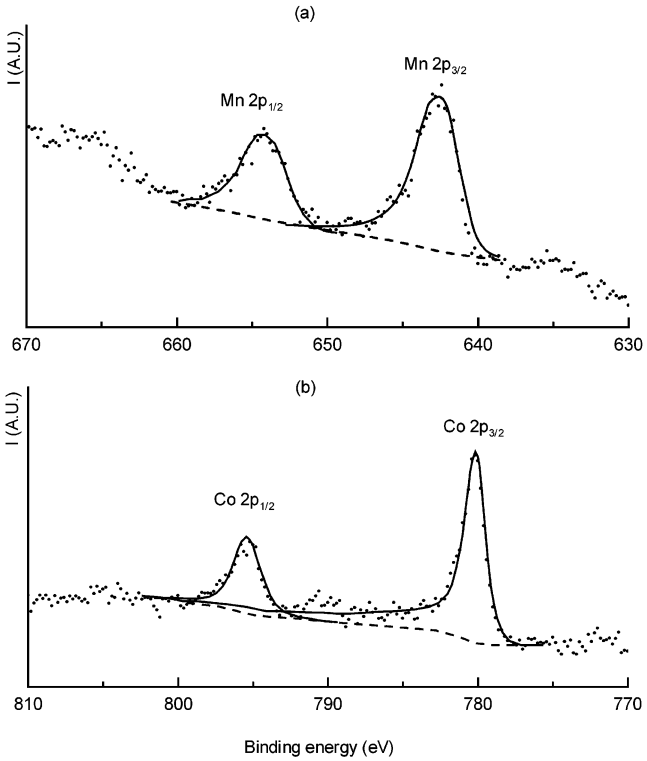

Figure 5. Comparison of the calculated XPS spectra (solid line) with the experimental data (points) for T#2-$Li_{2/3}Co_{2/3}Mn_{1/3}O_2$: Mn 2p (a) and Co 2p (b). Dotted line represents the background.

would be formed due to hygroscopicity of the sodium-containing phase. After the ion-exchange reaction the shape of the particles is not modified; it is still well-defined with only a few cracks on the edges. The size of the particles remains also similar after the ion-exchange reaction. Nevertheless, the surface of these particles appears cleaner, probably due to the washing of the carbonates with demineralized water after the ion-exchange reaction. The overall shape and size of the T#2-$Li_{2/3}Co_{2/3}Mn_{1/3}O_2$ crystallites are similar to those observed for the O2-$LiCoO_2$ and T#2-$Li_{2/3}Ni_{1/3}Mn_{2/3}O_2$ crystallites, also obtained by ion exchange of Na^+ by Li^+ in P2-type phases.[4,12]

Composition and Oxidation State Determination. Inductively coupled plasma (ICP) titration gave the composition $Li_{0.68}[Co_{0.67}Mn_{0.33}]O_2$ for the lithium-containing phase (the experimental percentages are Li = 5.0%, Co = 41.8%, and Mn = 19.3% whereas the theoretical percentages are Li = 4.9%, Co = 41.7%, and Mn = 19.4%, the oxygen stoichiometry being assumed to be 2), in good agreement with the exchange of 1 Li^+ for 1 Na^+ in P2-$Na_{2/3}Co_{2/3}Mn_{1/3}O_2$. To check the oxidation states of the Mn and Co ions, we have performed XPS experiments.

Figure 5a and 5b present the Mn and Co XPS spectra, with respectively the Mn $2p_{1/2}$−Mn $2p_{3/2}$ (654.0 and 642.6 eV) and the Co $2p_{1/2}$−Co $2p_{3/2}$ (795.0 and 780.1 eV) peaks, respectively. The binding energies were obtained by fitting the experimental curve. The calculated curve was defined by a combination of Gaussian and Lorentzian distributions with an anisotropic contribution. The latter was introduced to take into account the asymmetrical shape always observed for the transition metal 2p lines.[22] In the case of the cobalt core level, the spectrum shows the presence of Co^{3+} ions only. Indeed, the binding energy of 780.1 eV for the Co $2p_{3/2}$ peak is in good agreement with the value reported in the literature for Co^{III} ions (779.8 eV) in O3-$LiCo^{III}O_2$ compared to that for Co^{IV} ions (781.5 eV) in Li_x-$Co^{III,IV}O_2$.[23] Note that even if O3-$LiCoO_2$ and O3-Li_xCoO_2 are not isostructural to T#2-$Li_{2/3}Co_{2/3}Mn_{1/3}O_2$, they are also characterized by a layered structure with cobalt ions in oxygen octahedral environments. The displacement of the Co $2p_{3/2}$ peak depends thus only on the cobalt oxidation state. In the case of manganese, the values generally reported for the Mn $2p_{3/2}$ peak are 642.7 eV for Mn^{IV} in $LiMn^{III,IV}{}_2O_4$ and $Mn^{IV}O_2$ (pyrolusite) and 641.7 eV for Mn^{III} in $LiMn^{III,IV}{}_2O_4$ and $Mn^{III}{}_2O_3$ (bixbyite).[24] The experimental value of 642.6 eV obtained in our case fits rather well with Mn^{IV}. Because the binding energies of Mn^{IV} and Mn^{III} are rather close, we tried to fit the experimental data by taking into account the possible presence of the two oxidation states, but no significant amount of Mn^{III} was evidenced. The lithium-containing phase obtained by ion exchange of Na^+ by Li^+ in P2-$Na_{2/3}Co_{2/3}Mn_{1/3}O_2$ is thus characterized by the formula $Li_{2/3}[Co^{III}{}_{2/3}Mn^{IV}{}_{1/3}]O_2$, which was actually expected directly from the solid-state chemistry point of view.

It appears that during this ion-exchange reaction, 1 Na^+ is exchanged by 1 Li^+ in P2-$Na_{2/3}Co_{2/3}Mn_{1/3}O_2$, contrary to what occurs for O2-$LiCoO_2$. The lithium amount present in the final material depends on the oxidation states stable for the transition metal ions in the MO_2 slabs. Because the Co^{IV} ions are not stable, the formation of the O2-$LiCoO_2$ occurs through the reduction of Co^{IV} to Co^{III} and thus the exchange of 1 Li^+ for 2/3 Na^+.[4] On the contrary, the Ni and Mn ions are respectively stable in the +II and +IV oxidation states; the T#2-$Li_{2/3}Ni_{1/3}Mn_{2/3}O_2$ phase is thus formed with the exchange of 1 Li^+ for 1 Na^+ in P2-$Na_{2/3}Ni_{1/3}Mn_{2/3}O_2$. In the same way, the cobalt and manganese ions are respectively stable in the +III and +IV oxidation states; T#2-$Li_{2/3}Co_{2/3}Mn_{1/3}O_2$ is, therefore, stabilized with the exchange of 1 Li^+ for 1 Na^+ in P2-$Na_{2/3}Co_{2/3}Mn_{1/3}O_2$.

Rietveld Analysis of the Neutron Diffraction Data. A neutron diffraction study of T#2-$Li_{2/3}Co_{2/3}Mn_{1/3}O_2$ was performed to overcome the weak points of X-ray diffraction. Because the neutron scattering amplitude varies almost randomly throughout the periodic table, the lithium ions, with a Fermi length equal to $-1.9\ 10^{-13}$ cm, can be easily localized by using neutron diffraction in a cobalt-, manganese-, and oxygen-containing lattice (b(Co) = 2.5×10^{-13} cm, b(Mn) = -3.7×10^{-13} cm, and b(O) = -5.8×10^{-13} cm), whereas this is not possible by X-ray diffraction due to a very small X-ray scattering factor for lithium. Furthermore, close elements such as cobalt and manganese have very different Fermi lengths whereas they have very similar X-ray scattering factors: the opposite signs of their Fermi lengths would especially allow an easy observation of a possible Co/Mn ordering in the slabs.

(22) Briggs, D.; Seah, M. P. *Auger and X-ray Photoelectron Spectroscopy*; Wiley: New York, 1990.
(23) Dupin, J. C.; Gonbeau, D.; Martin-Litas, I.; Vinatier, P.; Levasseur, A. *J. Electron Spectrosc. Relat. Phenom.* **2001**, *120*, 55.
(24) Treuil, N.; Labrugère, C.; Ménétrier, M.; Portier, J.; Campet, G.; Deshayes, A.; Frison, J. C.; Hwang, S. J.; Song, S. W.; Choy, J. H. *J. Phys. Chem. B* **1999**, *103*, 2100−2106.

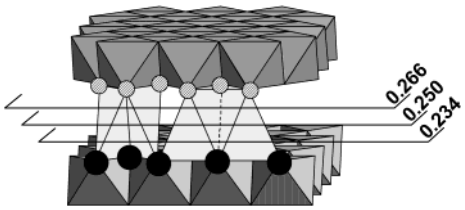

Figure 6. Perspective view of one-half of the $T^{\#}2$ unit cell along the $c_{orth.}$ axis, with two MO_2 slabs and in between the interslab space. The upper oxygen layer of the interslab space is represented by hatched circles and the lower by black circles. The positions of the different Fourier maps, calculated in planes perpendicular to the $c_{orth.}$ axis at $z = 0.234$, 0.250, and 0.266, are also represented.

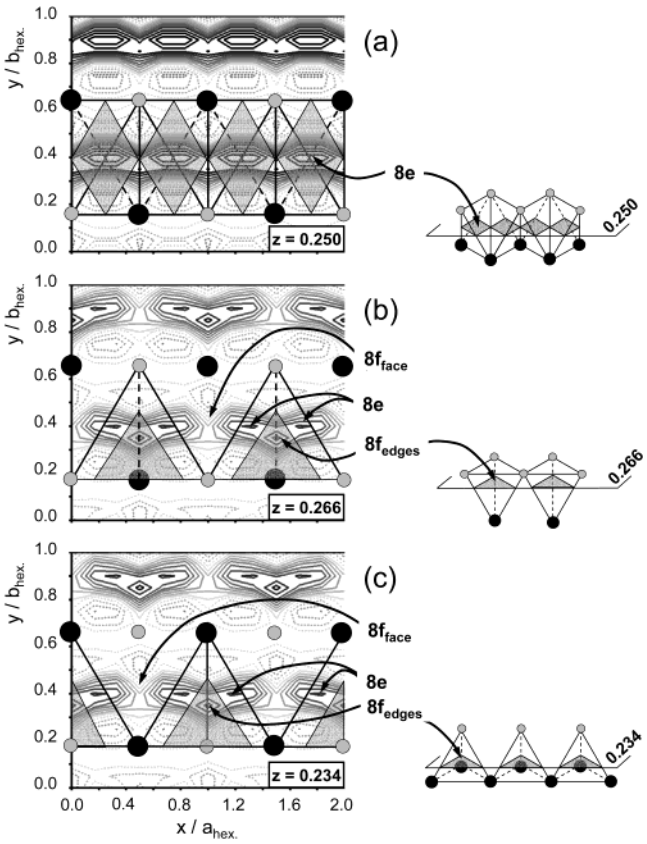

Figure 7. Nuclear density Fourier difference maps calculated in planes perpendicular to the $c_{orth.}$ axis at $z = 0.250$, 0.266, and 0.234 and the corresponding 3D perspectives showing the different tetrahedra linked along the x axis direction in the interslab space. The upper oxygen layer of the interslab space is represented by hatched circles and the lower by black circles. The projection of the tetrahedra is also reported in gray on the maps.

Contrary to what was observed for $T^{\#}2$-$Li_{2/3}[Ni_{1/3}Mn_{2/3}]O_2$ by Paulsen et al.,[18] no superstructure diffraction lines were observed for $T^{\#}2$-$Li_{2/3}Co_{2/3}Mn_{1/3}O_2$ in the range of small diffraction angles, showing that the Co^{3+} and Mn^{4+} ions are not ordered in the slabs. As currently observed, the driving force for the ordering is the difference in ionic radii and not the difference in cationic charge. In the case of the $T^{\#}2$-$Li_{2/3}[Ni_{1/3}Mn_{2/3}]O_2$ phase the difference in ionic radii ($r_i(Ni^{2+}) = 0.69$ Å and $r_i(Mn^{4+}) = 0.53$ Å) is high enough to lead to an ordering (tripling of the $a_{orth.}$ cell parameter[13]), while in the case of $T^{\#}2$-$Li_{2/3}Co_{2/3}Mn_{1/3}O_2$ phase the ionic radii are very similar ($r_i(Co^{3+}) = 0.545$ Å and $r_i(Mn^{4+}) = 0.53$ Å).[25]

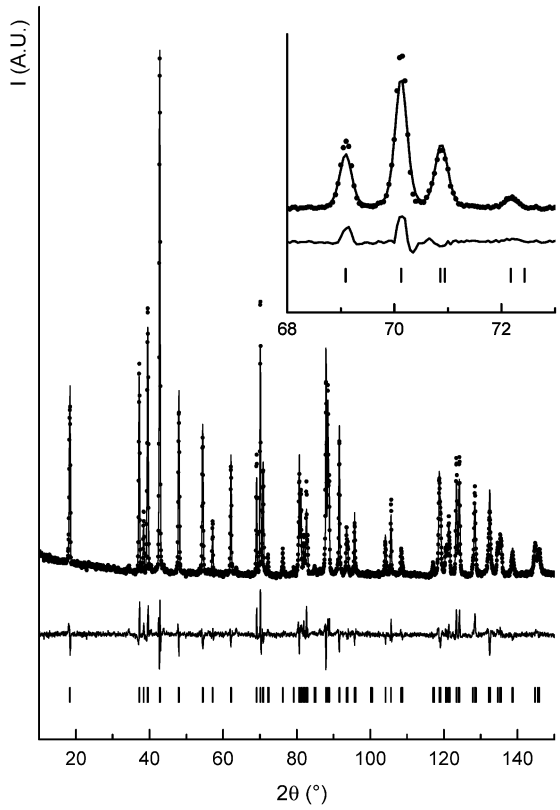

Figure 8. Comparison of the observed (●) and calculated (−) neutron diffraction patterns ($\lambda = 1.594$ Å) for $T^{\#}2$-$Li_{2/3}[Co_{2/3}Mn_{1/3}]O_2$. The positions of the ($hkl$) reflections and the difference curve are also given. An enlargement of the [68°−73°] 2θ range is shown in the insert.

In a first step, the host structure obtained from the XRD data was used for the refinement of the neutron diffraction data by the Rietveld method, all the structural parameters being fixed (i.e., $(Co_{2/3}Mn_{1/3})_{4a}(O_2)_{8f}$). The Co and Mn atoms were distributed in the 4a (0, 0, 0) position and the oxygen atoms in the 8f (0, ∼0.83, ∼0.60) position of the *Cmca* space group. The cell parameters and the coefficients of the pseudo-Voigt profile function were refined. The atomic displacement parameters (ADPs) of cobalt, manganese, and oxygen were fixed to 0.5 Å^2, a common value in that type of layered structures, and each site was constrained to be fully occupied. As expected (due to the missing lithium atoms in the structure), the minimization of the difference is obtained with high conventional Rietveld reliability factors, $R_{Bragg} = 10.1\%$ and $R_{wp} = 20.0\%$.

Figure 6 shows the perspective view of one-half of the $T^{\#}2$ unit cell along the $c_{orth.}$ axis, with two MO_2 slabs and in between one interslab space. The upper oxygen layer of the interslab space is represented by hatched circles and the lower by black circles. The positions of the different Fourier maps, calculated in planes perpendicular to the $c_{orth.}$ axis at $z = 0.234$, 0.250, and 0.266, are also shown in this figure: they were used to localize the lithium atoms in the structure. The nuclear density difference Fourier map obtained in the $z = 0.250$ plane is given in Figure 7a. The main residual nuclear density is clearly located at the ($^1/_4$, ∼0.40, $^1/_4$) position. As shown on the right side of Figure 7a, with the 3D

(25) Shannon, R. D.; Prewitt, C. T. *Acta Crystallogr.* **1969**, *B25*, 925.

Table 1. Structural Parameters Determined by the Rietveld Refinement of the Neutron Diffraction Data Recorded for T#2-$Li_{2/3}Co_{2/3}Mn_{1/3}O_2$[a]

space group: *Cmca*
$a_{orth.} = 2.8128(1)$ Å
$b_{orth.} = 4.8505(2)$ Å
$c_{orth.} = 10.0069(3)$ Å

atom	site	Wyckoff positions			occupancy	B (Å^2)
Li(1)	8e	1/4	0.41(3)	1/4	0.22(2)	2.1(6)
Li(2)	8f	0	0.8342(4)	0.266(5)	0.12(2)	2.1(6)
Co	4a	0	0	0	2/3	1.4(6)
Mn	4a	0	0	0	1/3	1.4(6)
O	8f	0	0.8342(4)	0.6012(3)	1	0.85(6)

Distances (Å)

d_{M-M}	2.80(1) ×4/2.81(1) ×2
d_{M-O}	1.91(1) ×4/1.91(2) ×2
$d_{Li_{8e}-O}$	2.10(2) ×2/2.00(2) ×2
$d_{Li_{8f_{edges}}-O}$	2.10(3) ×3/1.84(4) ×1

Conditions of the Run

temperature	300 K
angular range	$5° \le 2\theta \le 160°$
step scan increment (2θ)	0.04°
zero point (2θ)	−0.051(3)°
number of fitted parameters	21

Profile Parameters

pseudo-Voigt function
$PV = \eta L + (1 - \eta)G$ with $\eta = \eta_0 + X(2\theta)$

half-width parameters

$\eta_0 = 0.14(5)$
$X = 0.003(1)$
$U = 0.010(8)$
$V = -0.11(5)$
$W = 0.113(5)$

Conventional Rietveld *R*-factors for Points with Bragg Contribution
$R_{wp} = 15.5\%$; $R_B = 5.2\%$

[a] Note: Standard deviations have been multiplied by the Scor number (2.15) to correct from local correlations.

perspective view, this position corresponds to the center of the 8e tetrahedra. For $z = 0.266$ and $z = 0.234$, as shown in Figure 7b and 7c, the nuclear density difference Fourier maps calculated just above ($z = 0.266$) and just below ($z = 0.234$) the 8e sites reveal also residual nuclear density on the $8f_{edges}$ tetrahedral sites at the (1/2, ∼0.33, 0.266) and (0, ∼0.33, 0.234) positions (these two positions being equivalent and generated by the 8f (0, ∼0.83, 0.266) position). These $(LiO_4)_{8fedges}$ tetrahedra are represented with the 3D perspectives in Figure 7b and 7c and the corresponding projections are also given on the Fourier maps. As expected, due to face sharing with the MO_6 octahedra from the slabs, no residual nuclear density was observed in the $8f_{face}$ sites.

In a second step, we have added the lithium to the structural model considered for the Rietveld refinement; they were distributed on the 8e (1/4, ∼0.40, 1/4) and $8f_{edges}$ (0, ∼0.83, 0.266) sites. The parameters described previously were refined, but also the *y* and *z* atomic positions of oxygen, the *y* atomic position of lithium in the 8e site, the *y* and *z* atomic positions of lithium in the $8f_{edges}$ site, and all the atomic displacement parameters (ADPs), the ADPs of lithium being constrained to be the same on both sites and the sum of the occupancies on the 8e and $8f_{edges}$ sites being equal to 0.33 (in agreement with the $Li_{0.68}[Co_{0.67}Mn_{0.33}]O_2$ composition). The *y* atomic position of lithium in $8f_{edges}$ was constrained to be equal to that of the oxygen because the center of the tetrahedra associated to the $8f_{edges}$ site is localized vertically to the oxygen of the MO_2 slabs (Figure 2). The corresponding

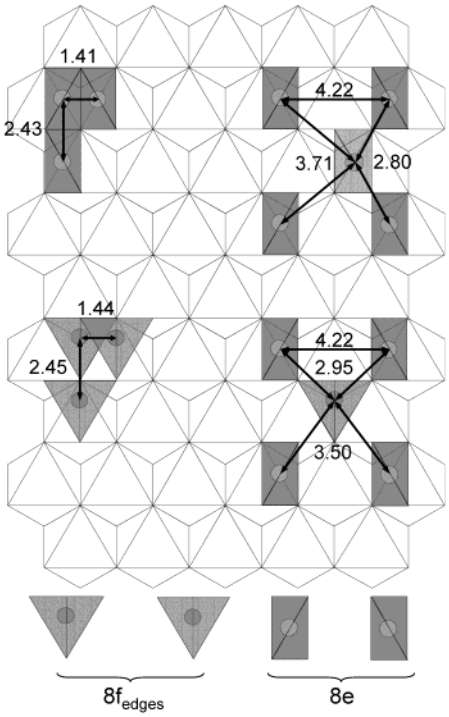

Figure 9. On the left side are reported the shortest distances between 8e (top) and $8f_{edges}$ (bottom) sites. On the right side are given distances between second neighbor 8e sites (top) and between second neighbor $8f_{edges}$ and 8e sites (bottom).

calculated and experimental diffractograms are represented in Figure 8. Results of this refinement are given in Table 1; they are in good agreement with those obtained for the Rietveld refinement of the X-ray diffraction data of the host structure. Introduction of lithium in the structure leads to a large decrease of the reliability factors and to a good minimization of the difference ($I_{obs.} - I_{calc.}$) ($R_{bragg} = 5.2\%$ and $R_{wp} = 15.5\%$). At this point, the nuclear density difference Fourier maps show no significant residual nuclear density.

The Rietveld refinement has shown that both 8e and $8f_{edges}$ sites were occupied by lithium, with the formula T#2-$\{(Li_{0.63})_{8e}(Li_{0.37})_{8f}\}_{2/3}[Co_{2/3}Mn_{1/3}]O_2$ for the lithium-containing phase. This result is in good agreement with the first-principles ab initio calculations made on T#2-Li_xCoO_2.[15] Indeed, it was shown that the occupancy of the $8f_{edges}$ was required by first-principles ab initio calculations to minimize the energy of the structures and to obtain a good agreement between the calculated and experimental galvanostatic curve of Li//Li_xCoO_2 in the composition range $0.52 < x \le 0.72$. The existence of two different sites for lithium for compositions such as $x > 0.5$ would allow the minimization of electrostatic repulsions in the lithium layers. Figure 9 shows the various lithium positions in the interslab space relative to the lower MO_2 slab. On the left side of the figure are given the shortest distances between 8e (top) or $8f_{edges}$ (bottom) sites. In all cases, the intersite distances are very short, preventing the simultaneous occupancy of two first neighboring sites, which is not required due to the very low Li^+/number of sites ratio. Therefore, only second neighbor sites are occupied (right of Figure 9). Considering the occupancy of the second neighbor sites, two Li^+ ion distribution can be considered. In the first one, where all the lithium ions are in the 8e site, this

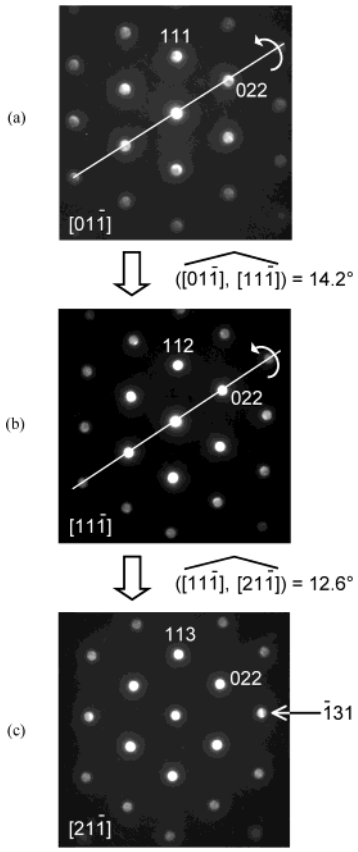

Figure 10. Electron diffraction patterns obtained for a crystal representative of the $T^{\#}2\text{-}Li_{2/3}[Co_{2/3}Mn_{1/3}]O_2$ sample and corresponding to (a) [01$\bar{1}$], (b) [11$\bar{1}$], and (c) [21$\bar{1}$] zone axes. Angles between the zone axes are also reported.

distribution leads to reasonable Li^+-Li^+ distances. Moving one lithium from an 8e to an $8f_{edges}$ site induces an increase of the shortest second neighbor distances from 2.80 to 2.95 Å, leading probably to a minimization of the Li^+-Li^+ electrostatic repulsions in the interslab space and thus to a better stabilization of the structure, even if simultaneously a decrease of the longest distances from 3.71 to 3.50 Å is observed. These intersite distances show that both 8e and $8f_{edges}$ sites can be simultaneously occupied as shown by the neutron diffraction study. Maybe the occupancy of the $8f_{edges}$ sites can be considered in relation to a high Li^+ diffusion in this structure, as suggested by an NMR study now in progress.

Transmission Electron Microscopy. To check if the distribution of lithium ions between two sites could be due to an ordering of lithium and vacancies in the interslab space, the $T^{\#}2\text{-}Li_{2/3}Co_{2/3}Mn_{1/3}O_2$ sample was studied by electron diffraction.[26,27] The electron diffraction patterns corresponding to the [01$\bar{1}$], [11$\bar{1}$], and [21$\bar{1}$] zone axes are shown in Figure 10. The second (b) and third (c) electron diffraction patterns were obtained by the rotation of the crystal around the [022] direction of the first pattern (a). Several crystals were studied; in all cases identical electron diffraction patterns were observed. All of them were indexed in the *Cmca* space group (the $\bar{1}31$ spot in Figure 10c is forbidden in the hexagonal $P6_3mc$ space group of the O2 structure) with cell parameters similar to those obtained from the neutron diffraction data ($a_{orth.} \approx 2.81$ Å, $b_{orth.} \approx 4.85$ Å, $c_{orth.} \approx 10.0$ Å). The full reconstruction of the reciprocal space shows no extra reflections; therefore, no ordering of the lithium ions in $T^{\#}2\text{-}Li_{2/3}Co_{2/3}Mn_{1/3}O_2$ exists.

This behavior is very different from what was observed in $T^{\#}2\text{-}Li_{0.7}CoO_2$, obtained by electrochemical deintercalation from $O2\text{-}LiCoO_2$, where superstructures spots probably due to lithium orderings in the interslab space were observed.[6] In $T^{\#}2\text{-}Li_{0.7}CoO_2$, the ordering of lithium ions is very easy because of the presence of one type of atom and the possibility of electronic transfer which do not inhibit the Li/□ ordering. On the contrary, for $T^{\#}2\text{-}Li_{2/3}Co_{2/3}Mn_{1/3}O_2$ phase, as there is no ordering of the Co^{3+} and Mn^{4+} ions in the slabs, the ordering of the lithium ions would be prevented in the interslab space.

Acknowledgment. The authors wish to thank Cathy Denage for the scanning electron microscopy analyses, Christine Labrugère for the XPS analyses, Emmanuelle Suard and Institut Laue-Langevin (ILL-Grenoble, France) for the neutron diffraction experiments, and CNES and Région Aquitaine for financial support.

CM035176P

(26) Pérès, J. P.; Weill, F.; Delmas, C. *Solid State Ionics* **1999**, *116*, 19−27.
(27) Shao-Horn, Y.; Weill, F.; Levasseur, S.; Delmas, C. *J. Electrochem. Soc.* **2003**, *150*, A366.